

Chapter

Redox Transitions in Pseudocapacitor Materials: Criteria and Ruling Factors

Sergey N. Pronkin, Nina Yu. Shokina and Cuong Pham-Huu

Abstract

Pseudocapacitance is a phenomenon of charge storage involving redox transitions at the electrode/electrolyte interface. As the result of an electrode potential modulation, one or few components of the electrode and/or electrolyte change its/their oxidation states. The redox reaction may be confined to the interface or propagate into the bulk of the electrode material, thus significantly increasing the charge (and energy) capacitance of the material. The rate and the reversibility of the interfacial redox reaction are the key factors determining the efficiency of charge storage due to pseudocapacitance phenomena. The influence of the characteristics of the interfacial redox reaction on the efficiency of charge storage in pseudocapacitive materials is considered in the current chapter. In particular, the similarities and the differences between the charge storage in batteries and pseudocapacitors are discussed. The analysis of the pseudocapacitive behavior of electrode material using the impedance spectroscopy is presented.

Keywords: pseudocapacitance, ion insertion, interfacial kinetics, impedance, staircase model

1. Introduction

The transition toward sustainable energy grids, based on renewable and non-critical resources, relies strongly on the technologies of efficient and reversible energy storage. Electrochemical energy storage devices (EESD) are among the most promising and versatile contemporary devices [1, 2]. Batteries, supercapacitors, and hybrid cells are the main classes of EESD, providing a wide range of energy and power densities. The energy densities of modern batteries are still inferior comparing to traditional (e.g., diesel) and modern (e.g., liquid hydrogen) fuels. However, high storage efficiency and zero operation emission make them indispensable elements of sustainable energy grids (**Table 1**).

Supercapacitors have ca. 10 times lower energy density comparing to batteries, but may operate at much higher power and have high capacitance retention with cycling. These differences are related to different mechanisms of charge storage in batteries and supercapacitors. Namely, in batteries the interfacial electrochemical reaction

Storage device	Energy density (W.h/kg)	Power density (W/kg)	Charge/discharge time	Cycles lifetime
Electrostatic capacitors	0.01–0.1	$> 10^5$	ms	∞
Supercapacitors	10–100	1000–10,000	From s to h	$> 10^4$
Li batteries	100–300	10–300	Hours	$\approx 10^3$
Diesel fuel	12,667	700 ^a	—	1
Liquid hydrogen	39,405	1500–2000 ^b	—	≈ 1000 h

^aIn standard V8 diesel engine.
^bIn PEMFC [3].

Table 1.
Energy and power density of various energy storage devices.

results in the transformation of the bulk of electrode materials. For example, in Li metal batteries, these reactions are the dissolution of Li to Li^+ at negative electrode and the intercalation of Li^+ to positive host electrode (e.g., graphite) [4]. While the maximal energy storage of batteries is primarily determined by the intercalation capacitance of host material, the power of energy input/output is limited by the rates of interfacial charge transfer and ion mass transport in solid-state bulk. Due to these factors, the energy capacitance of electrode materials in batteries strongly depends on the rate of charging.

On the other hand, in electrostatic capacitors, the charge Q is stored on two electrode plates separated by an insulator:

$$C = \frac{dQ}{dE} = \frac{\epsilon\epsilon_0}{d}A, \quad (1)$$

where $\epsilon_0 = 8.854 \cdot 10^{-12} \text{ F}\cdot\text{m}^{-2}$ is the vacuum permittivity, ϵ is the dielectric constant of the insulator, d is the distance between electrodes, and A is the surface area of the electrode.

Contrary to batteries, the capacitance of a capacitor does not depend on the rate of charging, providing that the charging time is longer than the circuit time constant $\tau = R_{ESR} \cdot C$, where R_{ESR} is the equivalent serial resistance of the circuit (**Figure 1A**).

In electrochemical capacitors, the charge is stored at or in the vicinity of the electrode/electrolyte interface (**Figure 1B**). Comparing to electrostatic capacitors, electrochemical capacitors have much shorter d (order of nm) and higher specific surface area (SSA) A per mass unit. Thus, electrochemical capacitor possesses, in general, the charge capacitance ca. 4 orders of magnitude higher than electrostatic capacitors.

From the practical point of view, it is useful to define various types of specific capacitance, as listed below.

- Surface specific capacitance $C_s = C/A$. According to (1), C_s depends only on the properties of the interface (d and ϵ).
- Mass specific (gravimetric) capacitance $C_g = C/m$. As a characteristic of supercapacitors, C_g is calculated per total mass of the device. However, in material science C_g is most often calculated per mass m of dry electrode material.

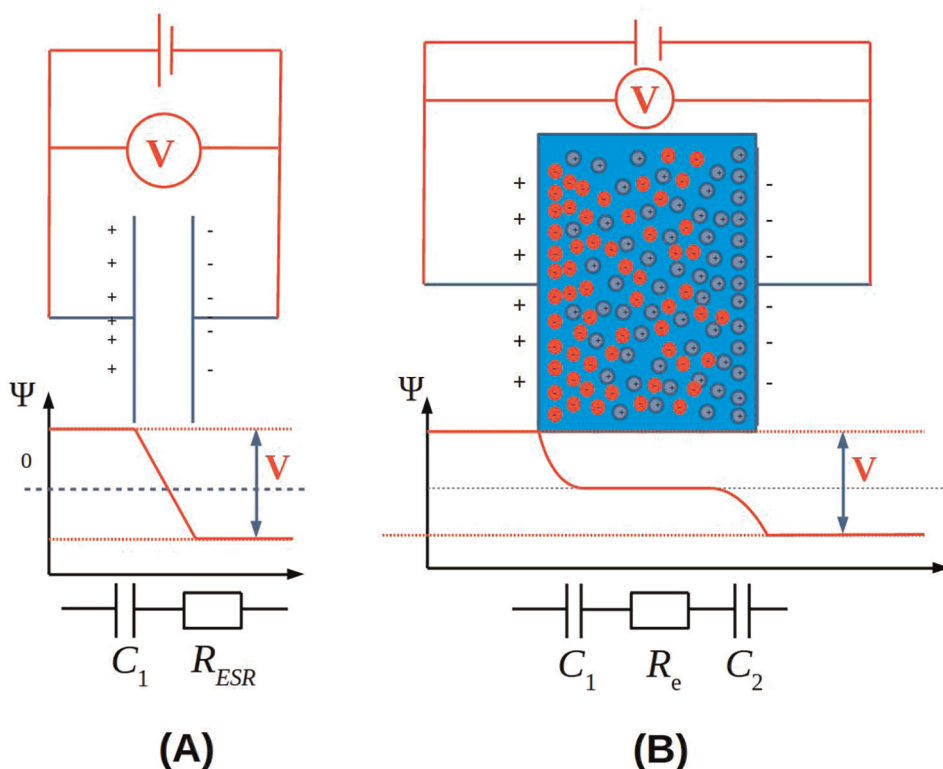


Figure 1. The scheme of distributions of the electrical potential between the electrodes of a solid-state capacitor (A) and an electrical double layer capacitor (B).

In this case, $C_g = C_s \cdot SSA$. C_g is a useful parameter for comparison of different electrode materials, because C_g depends on both interfacial charge storage efficiency (characterized by C_s) and material structure (characterized by SSA). However, this comparison can be misleading due to the utilization of dry material mass with pores filled by air. The efficient electrode material has an open porous structure with pores filled by electrolyte. It results in a significant increase in the mass of the electrode material. Thus, the true value of C_s is much lower than the value calculated with the mass of dry material.

- Volume specific capacitance $C_V = C/V$. Similarly to C_g , in material science the value of C_V is most often calculated using the volume unit of the electrode material V : $C_V = C_s \cdot SSA \cdot \rho$, where ρ is the density of a porous material. Contrary to C_g , C_V has the same value for dry material and material filled with an electrolyte. This is one of the reasons why C_V is a more relevant characteristics of the charge capacitance of the material than C_g [5].

Depending on the main mechanism of charge storage, one distinguishes between 2 types of supercapacitors: electrochemical double layer capacitors (EDLC) and pseudocapacitors.

As the name suggests, in EDLC main mechanism of charge storage is the formation of an electrical double layer at the electrode/electrolyte interface. In pseudocapacitors,

the predominant mechanism of charge storage is the pseudocapacitance phenomena. This phenomenon involves reversible interfacial electrochemical reaction and intercalation of a solvent component into the bulk of the electrode material. From the chemical point of view, the intercalation reactions in batteries and pseudocapacitors are similar. The important difference is that the rate of intercalation in supercapacitors, as opposed to batteries, is not limited by solid-state ion transport, but limited mostly by material intercalation capacitance and interfacial charge transfer rate.

In the current chapter, the influence of the rate of interfacial charge transfer on the electrochemical performance of electrode materials in supercapacitors is considered. The particular features of EDLC and pseudocapacitor performances are described. The focus of the current work is on the electrode materials of pseudocapacitors, because the charge transfer rate strongly influences the rate of pseudocapacitance phenomena. The influence of pseudocapacitance on the performance of EDLC is briefly discussed. The influence of interfacial charge transfer rate on the material capacitance of pseudocapacitors electrodes is first considered for a model flat electrode/electrolyte interface. Then, the dependence of the capacitance of porous electrode materials on interfacial charge transfer rate is analyzed. To evaluate the role of interfacial charge transfer, the models of interfacial impedance in the presence of pseudocapacitance reaction are considered.

2. The influence of the interfacial charge transfer rate on the performance of supercapacitors

2.1 Electrical double-layer capacitors

In EDLC the predominant mechanism of charge storage is charging of interfacial electrical double layer. This layer consists of adsorbed ions of electrolyte and solvent dipole molecules. The change of electrode potential results in changes of the ratio of adsorbed cations and anions at the interface and re-orientation of solvent dipoles. These phenomena result in charge accumulation at the interface with potential change, similarly to the charging of a capacitor when voltage is applied. The detailed models of the structure of the electrical double layer were developed in the last century [6]. As a very simple approximation, electrical double layer can be represented as a capacitor with one plate being an electrode and another plate being adsorbed ions and solvent molecules (**Figure 1B**). Under this approximation, the charge capacitance of the double layer C_{dl} is given by (1).

Considering that for aqueous solutions $\epsilon = 80$ and the thickness of electrical double layer is $d \approx 1$ nm, the surface specific charge capacitance C_s of electrode/electrolyte interface can be estimated as $C_s \approx 2 \cdot 10^{-5} \text{ F.cm}^{-2} = 20 \mu\text{F.cm}^{-2}$. A small thickness d of electrical double layer allows using the materials with highly developed surface as EDLC electrodes, for example, highly porous carbon materials with $\text{SSA} > 2600 \text{ m}^2.\text{g}^{-1}$ [7]. On the other hand, carbon/electrolyte interface has lower surface specific capacitance C_s comparing to metal/electrolyte interface, namely below $20 \mu\text{F.cm}^{-2}$ [8]. For a single-layer sp^2 carbon graphene sheet, the value of $13.5 \mu\text{F.cm}^{-2}$ is predicted and expected to decrease with the thickness of the carbon stack down to ca. $5 \mu\text{F.cm}^{-2}$ for the graphite structure. Thus, for carbon materials with highly developed SSA, the specific capacitance C_g related to double layer formation is expected to be in the range of 150–200 F/g.

The modulation of electrode potential results in the change of ion adsorption, solvent dipoles orientation, and, possibly, electrode surface reconstruction [9]. These phenomena lead to the changes of the values of d and ϵ of (1). Thus, the value of specific interfacial capacitance C_s may depend strongly on electrode potential. This results in the a complex shape of CV curves with well-defined CV peaks and different values of double layer charging current at different potentials.

However, these interfacial phenomena are relatively fast and the total charge associated with them does not depend on the rate of charging (rate of potential sweep). Therefore, the value of charging current is expected to be proportional to the rate of potential sweep for a given potential. This proportionality is one of the criteria that was proposed to distinguish between the electrode materials behaving as supercapacitor or battery electrode materials [10].

The surface-specific charge capacitance can be increased due to the phenomena of pseudocapacitance, which involves a fast and reversible surface electrochemical transformation of an electrode component at a certain potential. The following electrochemical phenomena may occur: oxidation/reduction of surface oxides, partial charge transfer to/from adsorbed electrolyte species (for example, electrochemical adsorption/desorption of atomic hydrogen [11], underpotential deposition of electrolyte metal cations [12]).

For carbon electrodes, the characteristic surface redox transformation is attributed to the presence of quinone-type surface groups on the partially oxidized surface [13, 14]. This reversible surface transition is reflected by the appearance of a pair of CV peaks around the equilibrium potential $E_0 = 0.668$ V (RHE) of quinone-hydroquinone redox couple. The surface density of quinone groups on oxidized carbon surfaces is estimated to be approximately equal to $0.1 - 1.1\%$ or $10^{-10} - 10^{-11}$ mol.cm⁻² [14]. These groups provide additional $1 - 10$ μF.cm⁻² to surface-specific capacitance. The interfacial capacitance is also increased in the presence of heteroatoms in carbon structure. In particular, an increase in surface charge capacitance due to N-doping of carbon was studied most thoroughly [15–18]. N-doping of carbon materials up to few %wt. can be achieved, resulting in a significant increase in surface specific capacitance. It allows to reach the mass specific capacitance close or even higher than 300 F/g for N-doped carbon electrode materials [17, 18].

As mentioned above, the predominant mechanism of charge storage in EDLC is a charging of an interfacial electrical double layer by ion adsorption and solvent molecule orientation, even though the surface pseudocapacitance phenomena may provide additional contributions. In contrast, in pseudocapacitors, the contribution of pseudocapacitance is predominant due to the propagation of the surface pseudocapacitance reaction further to the bulk of electrode material.

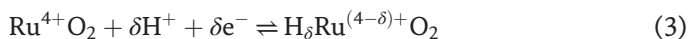
2.2 Pseudocapacitors

Even in the case of carbon materials, the pseudocapacitance reaction may propagate from interface further to the bulk of electrode material. One interesting example of this phenomenon is a hydrogen intercalation into a graphitic carbon structure. This phenomenon has been studied in details on activated carbon CH900–20 ACC (Japan) with SSA = 1520 m².g⁻¹ [19, 20]. Few hours of galvanostatic cathodic polarization of CH900–20 resulted in a formation of an intercalation compound with stoichiometry C₆H:



The maximal charge capacitance provided by the reaction (2) is 943 F/g, and the total mass specific capacitance C_g of CH900–20 in acid electrolytes is equal to 1114.3 F/g. To the knowledge of the authors, this is the highest mass-specific capacitance reported for carbon materials. On the other hand, the estimated diffusion coefficient D of hydrogen in carbon, according to [20] is estimated as $5 \cdot 10^{-17} \text{ cm}^2 \cdot \text{s}^{-1}$, and the intercalation is controlled by solid-state ion transport. This makes the material CH900–20 to be impractical for supercapacitors.

The pseudocapacitance is the main mechanism of charge storage in transition metal oxide (TMO) electrode materials commonly used as pseudocapacitor electrodes [21–23]. Similar to the functional groups at the carbon surface considered above, the metal cations at or in the vicinity of the electrode/electrolyte interface can undergo a fast reversible transformation due to a variability of oxidation states of transition metals. In comparison to the carbon, the percentage of metal sites available for the redox transformation is much higher: every metal atom is capable to change its oxidation state and participate in charge storage. This phenomenon provides significantly higher pseudocapacitance values for metal oxides comparing to carbon materials. The values above 900 F/g are routinely observed for RuO_2 -based electrode materials, which are among the best performing oxide materials in pseudocapacitors. As for the carbon electrodes, different phenomena can be involved in the pseudocapacitance: the surface redox transformation (involving interfacial charge transfer) and ion intercalation into solid-state electrode. For example, for RuO_2 , which is the most studied metal oxide supercapacitor material, the redox transition is described as follows [24]:



The transformation starts as an electroreduction of RuO_2 surface and then propagates into the bulk of the oxide. According to (3), this process can be also considered as H-intercalation. The transformation degree and the stored charge are characterized by the intercalation parameter δ : $0 \leq \delta \leq 1$.

In more general case, the reaction (3) can be presented as follows:



The nature of intercalating cation into the oxide materials from aqueous electrolytes is still debated even for Mn oxides—the second most studied type of oxides for supercapacitor electrodes. Most of transition metal oxides utilized in supercapacitor electrodes are stable only in neutral and alkaline solutions. Thus, the intercalation of cations of electrolyte (K^+ , Na^+) was proposed to be a pseudocapacitance reaction (4) [25, 26]. The inclusion of Na and S elements into thin film of MnO_2 and the decrease in Mn oxidation state from +4 to +3 (as the result of its polarization) have been indeed confirmed by ex situ XPS study [27]. However, the inclusion of these elements was mostly confined to the sub-surface atomic layers of oxide, while the high value of charge storage capacitance suggests the propagation of pseudocapacitance reaction into the bulk of oxide [27, 28]. Moreover, the pseudocapacitance reaction for Mn oxides appears to be pH-dependent: in general, higher charge capacitance is observed at higher pH [29, 30]. For $\text{Mn}_3\text{O}_4/\text{C}$ electrode material, the potential of pseudocapacitance reaction (4) was found to shift by 59 mV/pH (**Figure 2**).

These facts are more consistent with the nature of pseudocapacitance reaction of Mn oxides in aqueous solutions as expressed by the following equation:

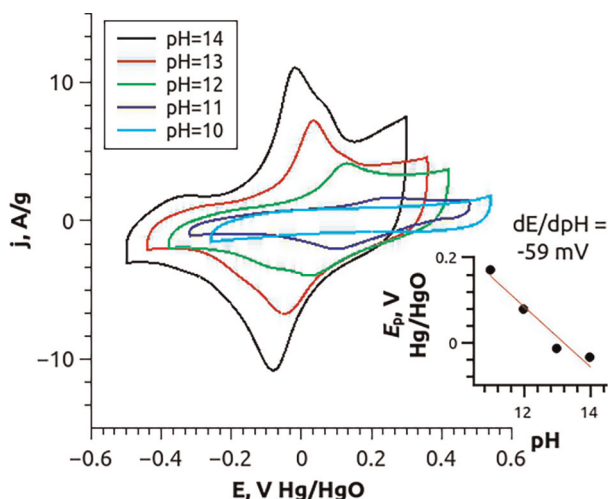
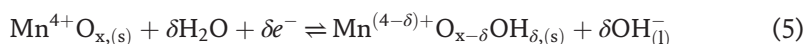


Figure 2. CV curves of Mn_3O_4/C (34%wt.) oxide electrode in 1 M ($Na_2SO_4 + NaOH$) electrolytes with various pH, measured at 20 mV/s [30].



The total specific amount of charge (in C/g) stored due to pseudocapacitance Q_{pc} is as:

$$Q_{pc} = \frac{x \cdot \delta \cdot F}{M}, \quad (6)$$

where x is the stoichiometric coefficient of metal cation in M_xO_y oxide, M is molecular weight of the oxide (in g/mol). For example, for RuO_2 , $Q_{cp} = 725.4$ C/g, according to (6), which is close to the experimental values of specific charge density $Q_C = 614$ C/g reported for amorphous RuO_2 [24]. This indicates that $\delta \approx 0.85$ for RuO_2 , i.e., the most of Ru cations in the bulk of the oxide are involved in the charge storage.

2.3 Pseudocapacitors versus batteries

The propagation of reaction (4) into the bulk of the oxide results in the cation Ct^+ intercalation into the oxide M_xO_y . Cation intercalation is also a charge storage mechanism in various types of batteries: in particular, the Li^+ cations are intercalated into the graphite cathodes in the conventional Li batteries [3]. The apparent similarities between these intercalation processes sparked the discussion about the criteria to distinguish between the materials behavior as battery or as supercapacitor electrodes [10, 31].

As discussed in Section 1, comparing to batteries, the pseudocapacitors provide smaller energy density storage, but operate with higher output power and better reversibility, i.e., retention of capacitance in a larger number of cycles. It suggests that the intercalation reaction is faster and more reversible in supercapacitors. The criteria of reversibility of intercalation reaction are considered below.

The rate of the reversible interfacial redox process of Ct^+ intercalation (4) is expressed by the equation [32], similar to the Butler-Volmer equation combined with the Frumkin isotherm:

$$i = i_0 \left((1 - \delta) e^{-(1-\alpha)g\delta} e^{\frac{(1-\alpha)F(E-E_0)}{RT}} - \delta e^{g\delta} e^{-\frac{\alpha F(E-E_0)}{RT}} \right). \quad (7)$$

Here i_0 is the exchange current density of reaction (4), α is the symmetry factor ($\alpha = 0.5$ for reversible intercalation). The constant g of the Frumkin isotherm characterizes the lateral interaction between the intercalated ions: $g < 0$ for attractive and $g > 0$ for repulsive interaction (most commonly observed for intercalation cations). For example, $g = -4.2$ was found for intercalation of Li^+ into Li_xCoO_2 [32].

The (7) assumes that the cations Ct^+ in the electrolyte and in the solid oxide phase are in quasi-equilibrium, which depends only on the interfacial potential E according to the Frumkin isotherm:

$$\frac{\delta}{1 - \delta} = e^{\frac{F(E-E_0)}{RT}} e^{-g(\delta-0.5)}. \quad (8)$$

Eqs. (7) and (8) assume that the distribution of δ within the bulk of host material is not influencing the interfacial reaction, i.e., that the rate of (4) is determined by its kinetics and not by the mass transport of Ct^+ in the solid phase. For example, for Li intercalation into LiCoO_2 , this model is valid at a potential sweep rate $10\text{--}50 \mu\text{V/s}$. At faster charging rates, the rate of Li^+ intercalation is determined by its diffusion in the host material and the Eqs. (7) and (8) are no longer valid.

Figure 3 illustrates the intercalation process of Ct^+ into the oxide particle and the formation of a gradient of Ct^+ concentration (or δ) within the particle. If $\delta_L \gg d$, where δ_L is a characteristic length of concentration gradient and d is the particle size,

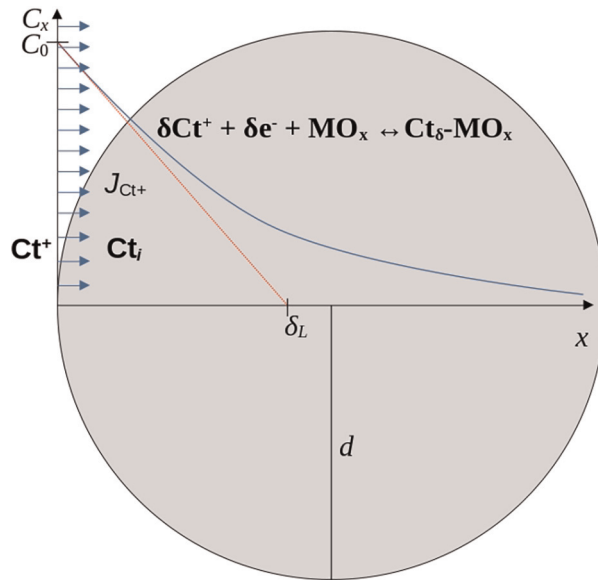


Figure 3.
The intercalation of Ct^+ into the oxide particle.

then the gradient of δ has no influence on the rate of interfacial reaction, the Eqs. (7) and (8) are valid, and the reaction (4) can be considered as reversible.

Assuming that the material of electrode has sufficiently high electronic conductivity, the presence of a gradient of potential inside the solid-state material can be neglected. Thus, the diffusion is a predominant mode of propagation of reaction (4) into the bulk of solid state. The solution of the first Fick's law for planar diffusion with boundary conditions $C_{\text{Ct}^+}{}_{x=0} = C_0$, $C_{\text{Ct}^+}{}_{x=\infty} = 0$ shows the relation between the current I of Ct^+ intercalation reaction (4) and the length of the concentration gradient δ_L :

$$I = AFC_0 \frac{D_{\text{Ct}^+}}{\delta_L}. \quad (9)$$

Here A is the surface area of the interface, D_{Ct^+} is the solid-state diffusion coefficient of Ct^+ . For an efficient intercalation host material, maximal value of δ is equal to 1 and C_{Ct^+} can be approximated as a concentration of metal cations at the interface, i.e. $C_{\text{Ct}^+} = C_0 \cdot \delta$. For example, for MnO_2 , $C_0 \approx \rho/M = 0.058 \text{ mol.cm}^{-3}$.

From the practical point of view, it is useful to relate the charging rate I (in A) with mass specific current density i_m (in A/g) by considering the geometry of a spherical particle with the diameter d :

$$i_m = \frac{6IA}{\rho d}, \quad (10)$$

where ρ is particles density (in g.cm^{-3}). Combining (9) and (10), the equation for the dependence of δ_L on i_m is obtained:

$$\delta_L = \frac{6FC_0\delta D_{\text{Ct}^+}}{i_m \rho d}. \quad (11)$$

Eq. (11) provides the criterion of reversibility of reaction (4). If $\delta_L \gg d$, then the concentration of intercalated cation within the oxide is nearly constant. In this case, the value of intercalation factor δ depends only on interfacial conditions, namely potential E , and the Eqs. (7) and (8) are valid. On the other hand, if $\delta_L \approx d$, then the value of intercalation factor δ depends on the distance from interface and is changing with time at constant E .

The strongest uncertainty in Eq. (11) is related to the values of solid-state diffusion coefficient D_{Ct^+} at ambient temperature. For Li batteries electrode materials, the values of D_{Li^+} are reported mostly for non-aqueous electrolytes. The values as high as $D_{\text{Li}^+}/C = 10^{-9} - 10^{-10} \text{ cm}^2.\text{s}^{-1}$ were determined for Li^+ intercalation into graphite electrode using impedance spectroscopy [33]. However, the values of Li^+ solid-state diffusion coefficients are most commonly found in the range $10^{-13} - 10^{-15} \text{ cm}^2.\text{s}^{-1}$ using the modeling of galvanostatic charging curves [34–36]. The advantages and limitations of this approach are thoroughly discussed in [37]. The thorough review of ambient temperature ionic conductivity in Li batteries electrode material is given in [38].

The diffusion coefficients D_{Ct^+} for cation intercalations from aqueous electrolytes are seldom measured. Indirectly, the values of D_{Ct^+} can be estimated from the ionic conductivity values of oxide σ_i using the following Equation [38]:

$$\sigma_i = \frac{F^2 C_{\text{Ct}^+} D_{\text{Ct}^+}}{RT}. \quad (12)$$

For example, for MnO₂ oxides, σ_i was reported in the range 0.001–0.02 Ohm⁻¹.cm⁻¹, depending on their crystallographic structure [39]. Thus, the diffusion coefficient values can be estimated as $D_{Ct^+} \approx 10^{-7} - 10^{-9}$ cm².s⁻¹ for a cation insertion into MnO₂ from aqueous electrolytes. In general, the rate of diffusion in supercapacitor electrode materials is expected to be few orders of magnitude larger comparing to Li⁺ diffusion in Li batteries electrode materials. Using the Eqs. (11) and (12), one may estimate δ_L value for 100 nm particles of a material with $\sigma_i = 0.001$ Ohm⁻¹.cm⁻¹: $\delta_L \approx 0.03$ cm even at fast charging rates ($i_m = 100$ A/g). Thus, for the oxide materials with relatively high ionic conductivity, $\delta_L \gg d$ even for fast charging rates. It indicates that the intercalation reaction can be considered as reversible and the material acts as a pseudocapacitor electrode.

The equations above provide qualitative criteria to distinguish between the materials behaving as supercapacitor or battery electrodes. To develop quantitative criteria, the modeling of various simultaneous interfacial processes as functions of their rates is needed. The simplest strategies for these models are considered below.

2.4 Impedance of flat interface in the presence of pseudocapacitance reaction

Impedance spectroscopy may provides detailed information of the interfacial phenomena occurring with various rates. In particular, in the presence of pseudocapacitance reaction on the flat electrode/electrolyte interface the following processes have to be taken into account.

- Formation of electrical double layer by reversible adsorption of electrolyte ions. Assuming a small amplitude of potential modulation, the interfacial characteristics (dielectric constant ϵ , change of ion adsorption with potential $d\Gamma/dE$) can be considered to be constant. The impedance of double layer formation is then expressed as a capacitance impedance:

$$Z_{dl} = -\frac{i}{\omega C_{dl}},$$

where $\omega = 2\pi f$ is the angular frequency (in rad/s), f is the potential modulation frequency (in Hz), C_{dl} is the double layer capacitance, $C_{dl} = C_s \cdot A$, where C_s is the surface specific capacitance (in F.cm⁻²), A is the electrode area (in cm²). Depending on the electrode material, C_s varies between 5 μ F.cm⁻² for carbon electrodes and 20–50 μ F.cm⁻² for metal electrodes.

- Interfacial charge transfer in the course of the reaction (4). For small potential modulations around the equilibrium redox potential E_0 , the Eq. (7) can be simplified to a linear form. The current i is proportional to the overvoltage $E - E_0$ and the impedance of this process can be approximated by a simple resistance R_{ct} :

$$Z_{ct} = R_{ct} = \frac{RT}{F \cdot i_0}.$$

- Diffusion of charged species into the bulk of the oxide material. Assuming the semi-infinite diffusion conditions ($C_{Ct^+,x=0} = C_0$, $C_{Ct^+,x=\infty} = 0$), the impedance of this process is given by the warburg impedance:

$$Z_W = \frac{\sigma}{\sqrt{\omega}} - \frac{i\sigma}{\sqrt{\omega}},$$

$$\sigma = \frac{RT}{\sqrt{2DA}F^2C_0}.$$

- Accumulation of charge in the bulk of oxide material. For small potential modulation this process can be considered similar to the accumulation of the charge at a capacitor:

$$Z_P = -\frac{i}{\omega C_p},$$

$$C_p = \frac{C_g \cdot A}{SSA \cdot 10^4}.$$

Here C_p is the capacitance of charge accumulation due to the pseudocapacitance reaction (in F), C_g is the gravimetric capacitance of electrode material (in F/g), SSA is the specific surface area of electrode material (in $\text{m}^2 \cdot \text{g}^{-1}$).

For a small potential modulation, the listed processes can be considered to be independent. In this case, the total interfacial impedance can be expressed by the Frumkin-Melik-Gaykazyan (FMG) model [32, 33], depicted as an equivalent circuit in **Figure 4**.

From the practical point of view, it is useful to correlate the frequency of the potential modulation f in the impedance spectra with the typical rates of potential variation during the charge/discharge of supercapacitors. The correlation can be done by using the root mean square rate v_{rms} of potential in the course of sinusoidal modulation:

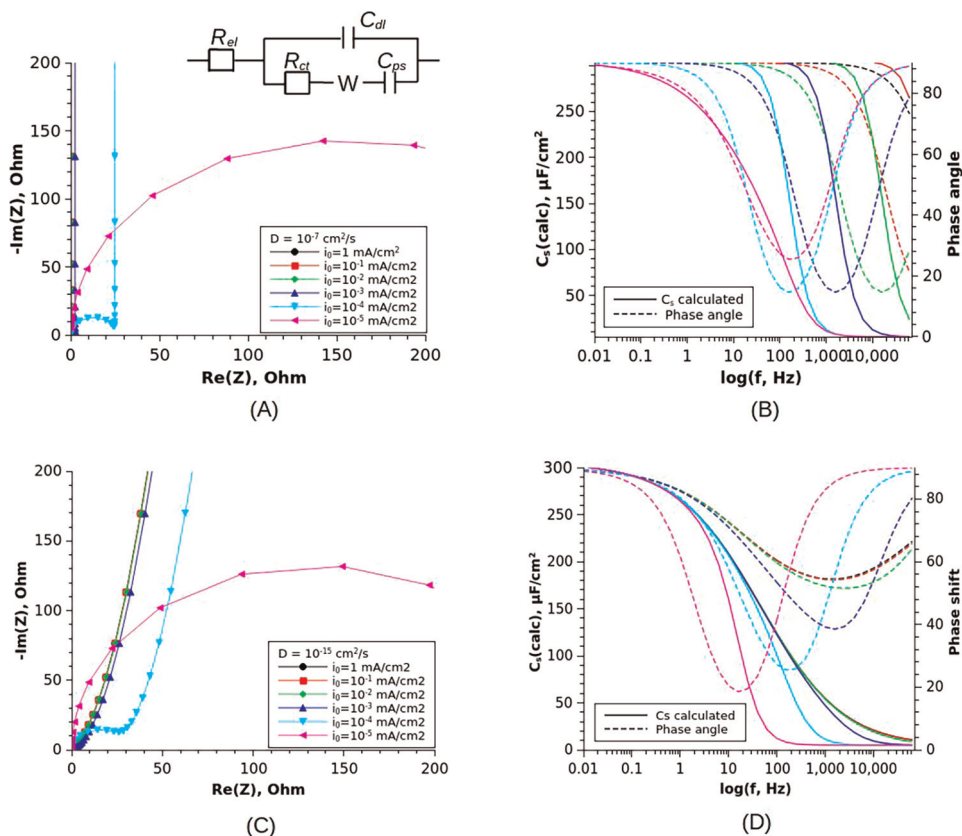
$$v_{rms} = \frac{2\pi E_0 f}{\sqrt{2}}, \quad (13)$$

where E_0 is the amplitude of potential modulation. One can demonstrate that 1C charging rate of a capacitor with 1 V operation voltage is comparable with the v_{rms} at $f = 6.25$ Hz (for $E_0 = 10$ mV). For 10C charging rate, the equivalent frequency is 62.5 Hz. Thus, one can roughly define the frequency range of interest for supercapacitors as ca. 0.1–10 Hz, and for batteries—below 1 Hz. This attribution is important for an interpretation of impedance modeling results.

Figure 4 shows the results of the modeling of interfacial impedance of a flat electrode in the presence of pseudocapacitance reaction, assuming $C_s = 5 \mu\text{F} \cdot \text{cm}^{-2}$, $C_g = 90 \text{ F} \cdot \text{g}^{-1}$, $SSA = 30 \text{ m}^2 \cdot \text{g}^{-1}$. The maximal surface specific capacitance of this interface is $C_m = 305 \mu\text{F} \cdot \text{cm}^{-2}$, consisting of both C_{dl} and C_p contributions. The Bode plots (**Figure 4B, D**) show the calculated values of the surface specific interfacial capacitance $C_{s,c}$ as a function of the modulation frequency and the rates of interfacial charge transfer i_0 and solid-state diffusion D . The values of $C_{s,c}$ are calculated from the calculated values of the interfacial impedance Z :

$$C_{s,c} = -\frac{1}{\omega \cdot \text{Im}(Z) \cdot A}. \quad (14)$$

As discussed above, the diffusion rate in supercapacitor electrode materials is few orders of magnitude larger comparing to Li batteries electrode materials. The


Figure 4.

Nyquist (A,C) and bode (B,D) plots for the Frumkin-Melik-Gaykazuan model of interfacial impedance in the presence of pseudocapacitance reaction, calculated for solid-state diffusion coefficients $D = 10^{-7} \text{ cm}^2 \cdot \text{s}^{-1}$ (A,B) and $D = 10^{-15} \text{ cm}^2 \cdot \text{s}^{-1}$ (C,D) and for various charge transfer rates (depicted in legend).

influence of the rate of solid-state diffusion on the behavior of the electrode materials can be illustrated by the comparison of the Bode plots calculated by the FMG model with $D = 10^{-7} \text{ cm}^2 \cdot \text{s}^{-1}$ for supercapacitors and with $D = 10^{-15} \text{ cm}^2 \cdot \text{s}^{-1}$ for batteries electrodes.

In the first case ($D = 10^{-7} \text{ cm}^2 \cdot \text{s}^{-1}$), for not particularly slow charge transfer rate ($i_0 > 10^{-4} \text{ mA} \cdot \text{cm}^{-2}$) C_s is frequency-independent and close to C_m . This behavior is observed in relatively wide frequency range at low and moderate frequencies ($f < 100 \text{ Hz}$). This shape of the Bode plots shows that the electrode material, including its bulk, acts as capacitor, while neither rate of charge transfer, nor rate of diffusion, are limiting factors of its charge/discharge. This is the set of conditions under which the material acts as a pseudocapacitor. Under these conditions, the amount δ of intercalated ions is determined by the interfacial equilibrium according to Frumkin isotherm (8), and depends only on the electrode potential. The phase angle of the interfacial impedance is close to $\phi = 90^\circ$ (dotted curves in **Figure 4B,D**). The Nyquist impedance plots under these conditions show straight vertical line with possible slight inclination due to the constant phase element behavior. The latter is often observed experimentally and explained by the capacitance slight dependence on applied frequency due to the surface heterogeneity, both chemical and geometrical [40, 41].

For very slow charge transfer rate ($i_0 \leq 10^{-5} \text{ mA.cm}^{-2}$), a clear decrease in C_s with an increase in f is expected even at low frequencies above 0.01 Hz, indicating that the material is not behaving as a pseudocapacitor even despite fast ionic transport in the solid-state.

At slow diffusion in solid state ($D = 10^{-15} \text{ cm}^2.\text{s}^{-1}$), the surface specific charge capacitance C_s decreases with increase in f even for fast charge transfer rates. In fact, the model curves for exchange rates $i_0 = 1 - 0.01 \text{ mA.cm}^{-2}$ are nearly identical, demonstrating that the rate of charging process is determined by a slow diffusion rate. For lower i_0 the decrease in C_s with increase in f becomes much sharper, as both diffusion and interfacial charge rates become limiting factors. As the amount δ of intercalated ions is limited by these factors, it is no longer in agreement with the Frumkin isotherm and the material cannot be considered as pseudocapacitor electrode material.

The described simple model is valid for flat interface only, because it neglects the effect of the geometry of electrode surface and material deposit. However, in EESD, such as batteries and supercapacitors, porous materials with well-developed interfacial surface area are utilized. To model the impedance of electrodes of supercapacitors, the influence of porous structure has to be taken into account.

2.5 Impedance of porous electrodes for supercapacitors

The interfacial impedance inside a pore is often modeled by the staircase-type equivalent circuit.

It was demonstrated that for the infinitely long cylindrical pore the interfacial impedance Z_p is described by the DeLevi Eq. (15) [42]:

$$Z_p = \sqrt{R|Z|}e^{i\frac{\phi}{2}}, \quad (15)$$

where R is the electrolyte resistance within the pore, Z is the impedance of a pore wall/electrolyte interface, and ϕ is the phase angle of Z . The Eq. (15) predicts that phase angle of the interfacial impedance of the pore is equal to a half of the phase angle of flat interface with the same characteristics. For example, the phase angle of the impedance of the interface with a double layer formation only is 90° for a flat interface, and 45° for the interface inside the infinite pore.

The behavior of the interfacial impedance of a porous system is determined by the penetration depth λ of potential modulation signal into the pore [43]:

$$\lambda = \frac{1}{2} \sqrt{\frac{\sigma d_p}{2\omega C_s}}, \quad (16)$$

here σ is the conductivity of the electrolyte, d_p is the pore diameter. The Eq. (16) suggests that at the frequency below a certain threshold f_0 , $\lambda > l_p$, where l_p is the length of the pore, and the whole surface of pore acts as a flat interface. Thus, the transition from infinite pore behavior to flat interface is observed on the impedance curves, that is often detected in the experiments with porous electrodes (for example [44]).

This staircase model allows to correctly fit experimental impedance spectra of porous electrodes in the absence of interfacial faradaic processes and determine the capacitance C_s . Moreover, the average pore length l_p can be estimated from the f_0

value, providing that the average diameter d_p of the pores is known from the other methods [45]. The model can also be adapted to take into account irregular shape of the pores: conical, globular pores etc. [43].

The majority of the studies of the impedance of porous systems simulate the pores as a system of parallel independent pores. The staircase circuit is applied separately to each pore, and total impedance is calculated as a parallel combinations of the pores. The supercapacitors electrode materials, for example the activated carbon, often have branching hierarchical structures: the larger pores are branching into few narrower pores of next generation, which can be branching further. The hierarchical porous structure of these materials makes the application of the staircase model more complicated, because the staircase circuits of pores from different generations are no longer independent.

The model of branching pores was proposed in [46] by introducing 2 generations of pores: the large (μm size) voids between carbon particles and the narrower (sub- μm size) internal pores. The larger pores were branching into n smaller pores with length and diameter scaled by a_l and a_d factors comparing to the parent pore. This model clearly demonstrated the influence of various parameters of geometry of pores on the performance of carbon materials in supercapacitors. An important conclusion of this work was the role of the interplay between the different parameters of the geometry. In particular, as the porosity of the material was a fixed parameter in the model, an increase in branching factor resulted in an increase in the diameter scaling factor, i.e., narrower pores of the next generation. As it follows from (16), the AC-penetration depth λ is shorter for an narrower pore, and, therefore, the utilization of an interface within such pore is less efficient. Thus, it was concluded that the branching of pores is counter-productive for their efficient utilization [46].

The staircase model was recently generalized take into account complexity of the porous structure of carbon electrode materials of supercapacitors [47]. Three generations of pores were considered: short and wide pores ($d_1 = 10 - 30$ nm) of the 1st generation were branching into β_{12} narrow mesopores of the 2nd generation ($d_2 = 3 - 10$ nm). The pores of the 2nd generation formed the main population of pores. These pores could also branch into β_{23} micropores ($d < 1$ nm). The branching was allowed to occur along the whole length of a parent pore. To take into account the contribution of pseudocapacitance, the Z_f interfacial impedance (see **Figure 5**) was

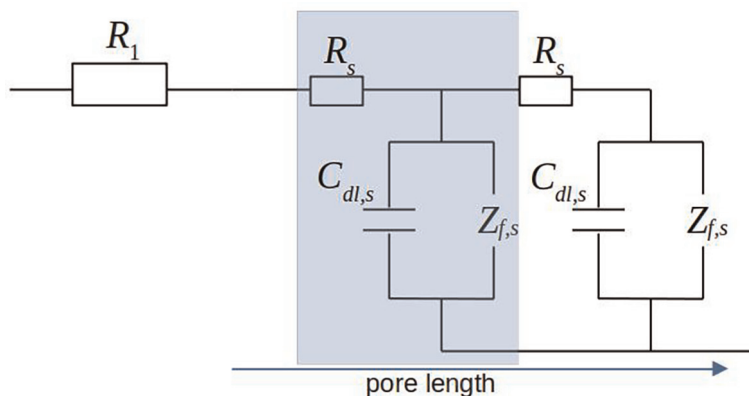


Figure 5. The staircase equivalent circuit of the impedance model inside a single pore. The highlighted elements form the repeating pattern along the pore.

modeled as a serial combination of charge transfer resistance R_{ct} and pseudocapacitance C_p . To limit the number of model parameters, relatively fast ion transport in the solid phase of the electrode was assumed. Thus, the warburg impedance Z_W was excluded from this model.

The Nyquist plots of the interfacial impedance, modeled by generalized staircase model in the absence of the faradaic impedance, are shown in **Figure 6A**. In agreement with simpler models, the curves show the transition from infinite pore behavior ($\phi = 45^\circ$) at high frequency to flat capacitor behavior ($\phi = 90^\circ$) at frequencies $f > f_0$. In the presence of the fast pseudocapacitance reaction ($i_0 = 0.1 \text{ mA/cm}^2$) and high pseudocapacitance ($C_p = 100 \text{ } \mu\text{F}\cdot\text{cm}^{-2}$), a characteristic semi-circular behavior is observed at intermediate frequencies (**Figure 6A,C**). The model also shows that the interfacial impedance changes significantly with the geometry of the electrode material for the same characteristics of pseudocapacitance reaction (**Figure 6A,C**).

One may distinguish between two main factors of the influence of the geometry of electrodes on the performance of electrode materials in supercapacitors: "penetration depth" (λ -factor) and "porosity" (ρ -factor). The λ -factor is related to the decrease in the value of λ with an increase in potential modulation frequency f (16). As the

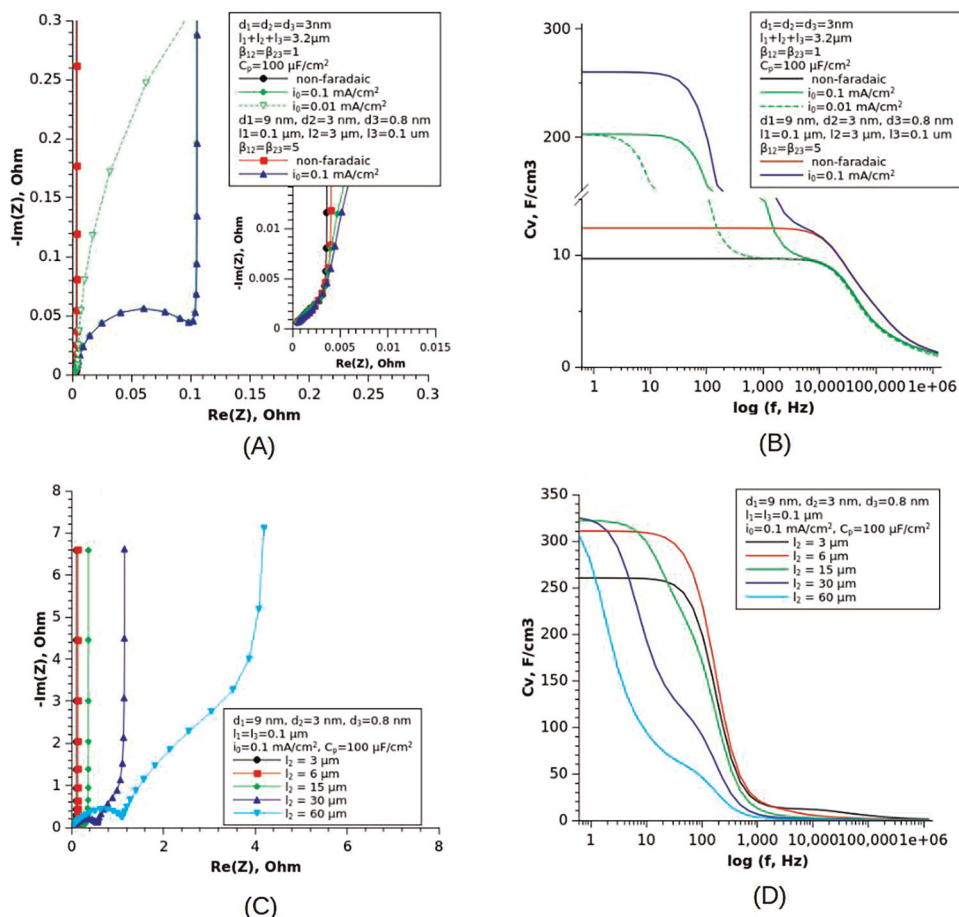


Figure 6. The Nyquist (A,C) and bode (B,D) plots for porous electrodes calculated by the generalized staircase model with 3 generations of pores. The non-faradaic model excludes Z_f from the calculations.

surface of "active" interface within the pores decreases, the interfacial capacitance C_s is also decreasing with increase in f , and this decrease is more pronounced for smaller and longer pores. On the other hand, smaller pores have lower inner volume and can provide high SSA while having lower porosity and higher density ρ of the material. Thus, these two factors are often found to be counter-active.

As it was mentioned above, the utilization of volume specific capacitance $C_V = C_s \cdot SSA \cdot \rho$ allows accounting for both λ - and ρ - factors. Similar to the previous section 2.4, C_s can be calculated from the model impedance values by (14). Similar to the model of flat interface (**Figure 4B,D**), the Bode plots for porous electrodes, constructed with C_V (**Figure 6B,D**), demonstrate flat segments at low frequencies, corresponding to $\phi = 90^\circ$, or pseudocapacitive behavior. The values of C_V of these segments are determined by ρ -factor: it is higher for smaller and longer pores. Also, the branching of the pores provides the material with higher density (fewer pore are needed for high SSA), and, thus, higher C_V values at low frequencies (**Figure 6B**).

However, comparing to flat interface, the segment of pseudocapacitive behavior is much shorter: the decrease in C_V with increasing frequency is observed at significantly lower frequencies. This decrease is related to λ -factor of geometry influence and it is more significant and observed at lower threshold f_0 for smaller and longer pores (**Figure 6D**).

For fast pseudocapacitance reaction ($i_0 = 0.1 \text{ mA}\cdot\text{cm}^{-2}$) and the typical porous structure of mesoporous carbon (predominant pores with $d \approx 3 - 10 \text{ nm}$ and $l \approx 1 - 3 \mu\text{m}$), the pseudocapacitive behavior is observed up to $f \approx 100 \text{ Hz}$, i.e., in the region of potential modulation rates relevant for supercapacitors. However, for slower reactions the range of pseudocapacitive behavior is limited to low-frequency ranges only ($f < 1\text{Hz}$), showing strong effect of λ -factor of the geometry of pores on the capacitance of electrode material. Also, for longer pores of few tens of μm (e.g., thick electrode deposits), the pseudocapacitive behavior is restricted to slow potential modulation even for very fast pseudocapacitance reaction (**Figure 6D**).

3. Conclusions

The phenomenon of pseudocapacitance allows to increase significantly the charge storage capacitance of the materials by involving the bulk of the electrode material to the charge storage. This phenomenon involves a fast and reversible interfacial charge transfer reaction, followed by an insertion of electrolyte cation into sub-surface and bulk layers of the solid-state electrode. This phenomenon is similar to cation intercalation into the batteries electrodes. However, in the case of supercapacitors, the interfacial reaction must be fast and reversible. In this case, the amount of inserted cation, as characterized by the intercalation factor δ , is in agreement with the Frumkin isotherm (8). In practical terms, this criterion means that the amount of stored charge depends only on the applied potential and does not depend on the rate of charging.

In the case of several simultaneous interfacial phenomena, the electrochemical behavior of the materials can be analyzed by interfacial impedance measurements and modeling. The advantage of the impedance spectroscopy is that, due to a small potential modulation, various interfacial phenomena can be considered to be independent and total impedance can be modeled as a combination of several elements corresponding to different processes. Namely, the impedance of flat electrode/electrolyte interface in the presence of pseudocapacitance phenomena can be analyzed by the FMG model. This analysis shows that in the case of relatively fast ion transport in

the solid phase ($D \approx 10^{-7} \text{ cm}^2 \cdot \text{s}^{-1}$) and not particularly slow interfacial charge transfer rates (i.e., $i_0 > 10^{-4} \text{ mA} \cdot \text{cm}^{-2}$), the pseudocapacitive behavior is expected up to very fast potential modulation ($f \approx 100 \text{ Hz}$). Under these conditions, the calculated surface specific interfacial capacitance C_s does not depend on the frequency f and the impedance phase angle is close to $\phi = 90^\circ$. This behavior is in clear contrast to the behavior of materials with slow ion transport in solid phase $D \approx 10^{-15} \text{ cm}^2 \cdot \text{s}^{-1}$, in which case a decrease in C_s with increase in potential modulation rate is detected already at low frequencies $f \approx 0.01 \text{ Hz}$ even for fast charge transfer rates ($i_0 = 0.1 \text{ mA} \cdot \text{cm}^{-2}$).

The analysis of the electrochemical behavior of electrode materials for supercapacitors must take into account the complex porous structure of these materials. For this purpose, the generalized staircase model of interfacial impedance for materials with hierarchical branching porous structure can be used. The effects of the geometry of pores on the performance of electrode materials of supercapacitors can be roughly categorized into two groups of factors. First, the presence of pores allows increasing significantly the specific surface area of the material, thus increasing the area of interface available for charge storage. The narrower pores with higher branching factors have lower inner volume, resulting in higher density of electrode material and, correspondingly, higher volume specific capacitance C_V . This group of effects is referred to as ρ -factors. The second group of effects, referred to as λ -factors, is related to the dependence of λ , i.e., penetration depth of potential modulation to the pore, on the potential modulation frequency f . The value of λ is shorter for narrower pores (16); thus ρ - and λ -factors are most often counter-active.

The modeling of the interfacial impedance of porous electrodes shows that the pseudocapacitive behavior (i.e., the values of C_s and C_V being independent on the potential modulation rate f) is confined to lower frequencies f due to λ -factors, comparing to flat interface. In particular, for thick deposits of mesoporous carbon, a decrease in interfacial capacitance with increase in f can be expected even for relatively fast interfacial charge transfer rate $i_0 \approx 0.01 \text{ mA} \cdot \text{cm}^{-2}$.

In general, one may conclude that in the case of flat electrodes of materials with sufficiently high ionic conductivity ($\sigma_i > 0.001 \text{ Ohm}^{-1} \cdot \text{cm}^{-1}$), the pseudocapacitive behavior of electrode materials can be observed even for moderate interfacial charge rates ($i_0 \geq 10^{-4} \text{ mA} \cdot \text{cm}^{-2}$). However, the materials with high SSA and developed porous structure are commonly employed in supercapacitors, which imposes stronger limitations on the rate of interfacial charge transfer. Thus, the demonstration of the pseudocapacitive behavior of a material with flat geometry of the interface is not sufficient to suggest its application in supercapacitors. The pseudocapacitive behavior has to be experimentally demonstrated and/or numerically simulated for the given material with porous structure.

Acknowledgements

Sergey Pronkin is indebted to ANR for the financial support of the project INFINE (ANR-21-CE08-0025, 2021-2024).

Conflict of interest

Authors declare no conflict of interests.

Abbreviations

EESD	Electrochemical energy storage device
CV	Cyclic voltammetry
SSA	Specific Surface Area
RHE	Reversible hydrogen electrode
TMO	Transition metal oxides
XPS	X-ray photoelectron spectroscopy
MFG	Frumkin-Melik-Gaykazyan (impedance model)

Author details


Sergey N. Pronkin^{1*}, Nina Yu. Shokina² and Cuong Pham-Huu¹

1 Institute of Chemistry and Processes for Energy, Environment, and Health (ICPEES UMR-7515 CNRS-Unistra), Strasbourg, France

2 University of Freiburg, Medical Center, Radiology Clinics, Freiburg, Germany

*Address all correspondence to: sergey.pronkin@unistra.fr

IntechOpen

© 2022 The Author(s). Licensee IntechOpen. This chapter is distributed under the terms of the Creative Commons Attribution License (<http://creativecommons.org/licenses/by/3.0>), which permits unrestricted use, distribution, and reproduction in any medium, provided the original work is properly cited. 

References

- [1] Grey CP, Tarascon JM. Sustainability and in situ monitoring in battery development. *Nature Materials*. 2016; **16**(1):45-56. DOI: 10.1038/nmat4777
- [2] Dühnen S, Betz J, Kolek M, Schmuch R, Winter M, Placke T. Toward green battery cells: Perspective on materials and technologies. *Small Methods*. 2020; **4**(7):2000039. DOI: 10.1002/smt.202000039
- [3] Mock P, Schmid SA. Fuel cells for automotive powertrains — A techno-economic assessment. *Journal of Power Sources*. 2015; **190**(2009):133-140. DOI: 10.1016/j.jpowsour.2008.10.123
- [4] Tarascon JM, Armand M. Issues and challenges facing rechargeable lithium batteries. *Nature*. 2001; **414**(6861): 359-367. DOI: 10.1038/35104644
- [5] Gogotsi Y, Simon P. True performance metrics in electrochemical energy sources. *Science*. 2011; **334** (January):917-918. DOI: 10.1126/science.1213003
- [6] Parsons R. Electrical double layer – Recent experimental and theoretical developments. *Chemical Reviews*. 1990; **90**:813-826
- [7] Zhang LL, Zhou R, Zhao XS. Carbon-based materials as supercapacitor electrodes. *Journal of Materials Chemistry*. 2009; **38**(29):2520-2531. DOI: 10.1039/c000417k
- [8] Ji H, Zhao X, Qiao Z, Jung J, Zhu Y, Lu Y, et al. Capacitance of carbon-based electrical double-layer capacitors. *Nature Communications*. 2014; **5**(3317):1-7. DOI: 10.1038/ncomms4317
- [9] Pajkossy T, Wandlowski T, Kolb DM. Impedance aspects of anion adsorption on gold single crystal electrodes. *Journal of Electroanalytical Chemistry*. 1996; **414**(2):209-220. DOI: 10.1016/0022-0728(96)04700-6
- [10] Simon P, Gogotsi Y, Dunn B. Where do batteries end and supercapacitors begin? *Science*. 2014; **343**(6176): 1210-1211. DOI: 10.1126/science.1249625
- [11] Jerkiewicz G. Electrochemical hydrogen adsorption and absorption. Part 1: Under-potential deposition of hydrogen. *Electrocatalysis*. 2010; **1**(4): 179-199. DOI: 10.1007/s12678-010-0022-1
- [12] Herrero E, Buller LJ, Abruña HD. Underpotential deposition at single crystal surfaces of Au, Pt, Ag and other materials. *Chemical Reviews*. 2001; **101**(7):1897-1930. Available from: <http://www.ncbi.nlm.nih.gov/pubmed/11710235>
- [13] Noked M, Soffer A, Arubach D. The electrochemistry of activated carbonaceous materials: Past, present, and future. *Journal of Solid State Electrochemistry*. 2011; **15**(7-8):1563-1578. DOI: 10.1007/s10008-011-1411-y
- [14] Kinoshita K, Bett JAS. Potentiodynamic analysis of surface oxides on carbon blacks. *Carbon*. 1973; **11**(4):403-411. DOI: 10.1016/0008-6223(73)90080-8
- [15] Borenstein A, Hanna O, Attias R, Luski S, Brousse T, Aurbach D. Carbon-based composite materials for supercapacitor electrodes: A review. *Journal of Materials Chemistry A*. 2017; **5**(25):12653-12672. DOI: 10.1039/c7ta00863e
- [16] Mostazo-López MJ, Ruiz-Rosas R, Morallón E, Cazorla-Amorós D.

- Generation of nitrogen functionalities on activated carbons by amidation reactions and Hofmann rearrangement: Chemical and electrochemical characterization. In: Carbon. Vol. 91. Amsterdam, Netherlands: Elsevier; 2015. pp. 252-265. DOI: 10.1016/j.carbon.2015.04.089
- [17] Frackowiak E, Lota G, Machnikowski J, Vix-Guterl C, Béguin F. Optimisation of supercapacitors using carbons with controlled nanotexture and nitrogen content. *Electrochimica Acta*. 2006;**51**(11):2209-2214. DOI: 10.1016/j.electacta.2005.04.080
- [18] Wang R, Lang J, Yan X. Effect of surface area and heteroatom of porous carbon materials on electrochemical capacitance in aqueous and organic electrolytes. *Science China Chemistry*. 2014;**57**(11):1570-1578. DOI: 10.1007/s11426-014-5123-x
- [19] Volkovich YM, Bograchev DA, Mikhalin AA, Bagotsky VS. Supercapacitor carbon electrodes with high capacitance. *Journal of Solid State Electrochemistry*. 2014;**18**(5):1351-1363. DOI: 10.1007/s10008-013-2271-4
- [20] Volkovich YM, Bograchev DA, Rychagov AY, Sosenkin VE, Chaika MY. Supercapacitors with carbon electrodes. Energy efficiency: Modeling and experimental verification. *Journal of Solid State Electrochemistry*. 2015;**19**(9): 2771-2779. DOI: 10.1007/s10008-015-2804-0
- [21] Simon P, Gogotsi Y. Materials for electrochemical capacitors. *Nature Materials*. 2008;**7**(11):845-854. DOI: 10.1038/nmat2297
- [22] Wang G, Zhang L, Zhang J. A review of electrode materials for electrochemical supercapacitors. *Chemical Society Reviews*. 2012;**41**(2): 797-828. DOI: 10.1039/c1cs15060j
- [23] González A, Goikolea E, Barrena JA, Mysyk R. Review on supercapacitors: Technologies and materials. *Renewable and Sustainable Energy Reviews*. 2016;**58**: 1189-1206. DOI: 10.1016/j.rser.2015.12.249
- [24] Zheng JP. The limitations of energy density for electrochemical capacitors. *Journal of the Electrochemical Society*. 1997;**144**(6):2026. DOI: 10.1149/1.1837738
- [25] Wei W, Cui X, Chen W, Ivey DG. Manganese oxide-based materials as electrochemical supercapacitor electrodes. *Chemical Society Reviews*. 2011;**40**(3):1697-1721. DOI: 10.1039/C0CS00127A
- [26] Tsumura T, Tsumori K, Shimizu G, Toyoda M. Electrochemical properties of spinel-type manganese oxide/porous carbon nanocomposite powders in 1 M KOH aqueous solution. *Journal of Physics and Chemistry of Solids*. 2012;**73**(2): 237-244. DOI: 10.1016/j.jpics.2011.10.036
- [27] Toupin M, Brousse T, Bélanger D. Charge storage mechanism of MnO₂ electrode used in aqueous electrochemical capacitor. *Chemistry of Materials*. 2004;**16**(16):3184-3190. DOI: 10.1021/cm049649j
- [28] Zhang LL, Wei T, Wang W, Zhao XS. Manganese oxide-carbon composite as supercapacitor electrode materials. *Microporous and Mesoporous Materials*. 2009;**123**(1-3):260-267. DOI: 10.1016/j.micromeso.2009.04.008
- [29] Xie X, Gao L. Characterization of a manganese dioxide/carbon nanotube composite fabricated using an in situ coating method. *Carbon*. 2007;**45**(12): 2365-2373. DOI: 10.1016/j.carbon.2007.07.014
- [30] Kéranguéven G, Faye J, Royer S, Pronkin SN. Electrochemical properties

and capacitance of Hausmannite Mn_3O_4 – Carbon composite synthesized by in situ autocombustion method. *Electrochimica Acta*. 2016;**222**:755-764. DOI: 10.1016/j.electacta.2016.11.032

[31] Brousse T, Bélanger D, Long JW, Belanger D, Long JW. To be or not to be pseudocapacitive? *Journal of the Electrochemical Society*. 2015;**162**(5): A5185-A5189. DOI: 10.1149/2.0201505jes

[32] Levi MD, Aurbach D. Frumkin intercalation isotherm - a tool for the description of lithium insertion into host materials: A review. *Electrochimica Acta*. 1999;**45**(1):167-185. DOI: 10.1016/S0013-4686(99)00202-9

[33] Levi MD, Aurbach D. Diffusion coefficients of lithium ions during intercalation into graphite derived from the simultaneous measurements and modeling of electrochemical impedance and potentiostatic intermittent titration characteristics of thin graphite electrodes. *Journal of Physical Chemistry B*. 1997;**101**(23):4641-4647. DOI: 10.1021/jp9701911

[34] Prosini PP, Lisi M, Zane D, Pasquali M. Determination of the chemical diffusion coefficient of lithium in $LiFePO_4$. *Solid State Ionics*. 2002;**148**(1-2):45-51. DOI: 10.1016/S0167-2738(02)00134-0

[35] Ding N, Xu J, Yao YX, Wegner G, Fang X, Chen CH, et al. Determination of the diffusion coefficient of lithium ions in nano-Si. *Solid State Ionics*. 2009;**180**(2-3):222-225. DOI: 10.1016/j.ssi.2008.12.015

[36] Delacourt C, Ati M, Tarascon JM. Measurement of lithium diffusion coefficient in Li y $FeSO_4$ F. *Journal of the Electrochemical Society*. 2011;**158**(6):A741-A749. DOI: 10.1149/1.3581087

[37] Nickol A, Schied T, Heubner C, Schneider M, Michaelis A, Bobeth M, et al. GITT analysis of lithium insertion cathodes for determining the lithium diffusion coefficient at low temperature: Challenges and pitfalls. *Journal of the Electrochemical Society*. 2020;**167**(9):090546. DOI: 10.1149/1945-7111/ab9404

[38] Park M, Zhang X, Chung M, Less GB, Sastry AM. A review of conduction phenomena in Li-ion batteries. *Journal of Power Sources*. 2010;**195**(24):7904-7929. DOI: 10.1016/j.jpowsour.2010.06.060

[39] Ghodbane O, Pascal JL, Favier F. Microstructural effects on charge-storage properties in MnO_2 -based electrochemical supercapacitors. *ACS Applied Materials and Interfaces*. 2009;**1**(5):1130-1139. DOI: 10.1021/am900094e

[40] Kerner Z, Pajkossy T. On the origin of capacitance dispersion of rough electrodes. *Electrochimica Acta*. 2000;**46**(2-3):207-211. DOI: 10.1016/S0013-4686(00)00574-0

[41] Alexander CL, Tribollet B, Vivier V, Orazem ME. Contribution of surface distributions to constant-phase-element (CPE) behavior: 1. Influence of roughness. *Electrochimica Acta*. 2017;**251**:416-424. DOI: 10.1016/j.electacta.2017.08.081; Alexander CL, Tribollet B, Vivier V, Orazem ME. Contribution of surface distributions to constant-phase-element (CPE) behavior: 2. Capacitance. *Electrochimica Acta*. 2017;**251**:566-573. DOI: 10.1016/j.electacta.2017.08.081; Alexander CL, Tribollet B, Vivier V, Orazem ME. Contribution of surface distributions to constant-phase-element (CPE) Behavior: 3. Adsorbed intermediates. *Electrochimica Acta*. 2017;**251**, 99-108. DOI: 10.1016/j.electacta.2017.08.081

[42] MacDonald DD. Reflections on the history of electrochemical impedance spectroscopy. *Electrochimica Acta*. 2006;**51**(8–9):1376-1388. DOI: 10.1016/j.electacta.2005.02.107

[43] Keiser H, Beccu KD, Gutjahr MA. Abschätzung der Porenstruktur poröser Elektroden aus Impedanzmessungen. *Electrochimica Acta*. 1976;**21**(8):539-543. DOI: 10.1016/0013-4686(76)85147-X

[44] Ba H, Wang W, Pronkin S, Romero T, Baaziz W, Nguyen-Dinh L, et al. Biosourced foam-like activated carbon materials as high-performance supercapacitors. *Advanced Sustainable Systems*. 2018;**1700123**:1700123. DOI: 10.1002/adsu.201700123

[45] Kötz R, Carlen M. Principles and applications of electrochemical capacitors. *Electrochimica Acta*. 2000;**45**:2483-2498

[46] Eikerling M, Kornyshev AA, Lust E. Optimized structure of nanoporous carbon-based double-layer capacitors. *Journal of the Electrochemical Society*. 2005;**152**(1):E24-E33. DOI: 10.1149/1.1825379

[47] Pronkin SN, Shokina NY. Generalized staircase model of electrochemical impedance of pores in supercapacitor electrodes. *Computational Technologies*. 2021;**26**(5):30-51. DOI: 10.25743/ict.2021.26.5.004